Trans-Atlantic Field Trial Using High Spectral Efficiency Probabilistically Shaped 64-QAM and Single-Carrier Real-Time 250-Gb/s 16-QAM

Junho Cho, *Member, IEEE*, Xi Chen, *Member, IEEE*, Sethumadhavan Chandrasekhar, *Fellow, IEEE, Fellow, OSA*, Gregory Raybon, *Fellow, IEEE, Fellow, OSA*, Ronen Dar, Laurent Schmalen, *Senior Member, IEEE*, Ells Burrows, Andrew Adamiecki, Steve Corteselli, Yan Pan, Diego Correa, Brad McKay, Szilard Zsigmond, Peter J. Winzer, *Fellow, IEEE, Fellow, OSA*, and Steve Grubb

(Post-Deadline Paper)

***Abstract*—We report the transmission of probabilistically shaped (PS) 64-ary quadrature amplitude modulation (QAM) at 7.46 b/s/Hz over a 5523-km in-service trans-Atlantic fiber-optic cable that consists of 65–89-km spans of Erbium-doped fiber amplifier only amplified fiber. Using a looped-back system configuration, we achieve 5.68 b/s/Hz over a trans-Pacific-equivalent distance of 11 046 km. Net spectral efficiencies are increased by 18% and 80% by using PS, at 5523 km and 11 046 km, respectively, compared to uniform square QAM. Throughout our experiments, we pay particular attention that our claims are backed by implementable forward error correction schemes. In addition, we demonstrate real-time coherent transmission of single-carrier 200 and 250-Gb/s uniform 8-QAM and 16-QAM at 4 b/s/Hz over the 5523-km cable.**

***Index Terms*—Coherent detection, field trial, modulation, probabilistic constellation shaping, submarine transmission.**

I. Introduction

THE exponential growth of global data traffic driven by cloud-based applications has attracted significant attention from operators of web-scale cloud platforms to build their own intercontinental submarine fiber-optic cables [1]. Web-scale companies are investing in at least 106,460 km of submarine fiber-optic cables that are deployed between 2010 and 2018 [2], including the trans-Atlantic AEC-1 cable between Shirley, New York, USA, and Killala, Ireland, which began service in January 2016 [3], the trans-Atlantic MAREA cable between Virginia Beach, Virginia, USA, and Bilbao, Spain, whose initial service is planned for the 1st quarter of 2018, and the trans-Pacific PLCN cable between Manhattan Beach, California, USA, and Tseung Kwan O, Hong Kong, which will begin service in May 2018, on all of which Facebook operates or will operate on dedicated fibers [2].

Once deployed, it is crucial to maximize cable capacity through best-in-class transponders across the industry, in the spirit of open submarine line systems. The capacity of legacy submarine cables designed for past-generation technologies such as on-off keying and dispersion-managed fibers that commonly provide uneven channel qualities across the optical spectrum is also upgraded by latest coherent-optical transponders [4], since laying new submarine cables is extremely costly and time-consuming.

Both on the most advanced cables with minimum quality variations across wavelength division multiplexed (WDM) channels and on legacy cables with large channel-to-channel quality variations, *rate-adaptable coded modulation* is an essential technology to achieve maximum cable capacity. In today's most advanced commercial systems, rate adaptation is substantially limited to the ability to coarsely switch between a handful of predefined quadrature amplitude modulation (QAM) formats, such as binary and quadrature phase shift keying (BPSK, QPSK), 8-QAM, 16-QAM, and 64-QAM [5]. Recently, however, probabilistically shaped (PS) QAM re-emerged within the research community, offering a very fine granularity of information rates (IRs) and hence the ability to dynamically adapt the transponder to the physical channel on a per-wavelength basis [6]– [10].

Previous submarine field trials have reported 125 Gb/s per carrier over 4,108 km [11] and 200 Gb/s per carrier over 6,577 km [12] using off-line processing, but not in a fully-loaded dense WDM (DWDM) context, and without rate adaptability. In laboratory recirculating loops, fully-loaded DWDM experiments have achieved spectral efficiencies (SEs) of 8.3 b/s/Hz over 6,375 km on 56-km spans of hybrid 'quasi-single-mode' and 150-μm^2 effective area fiber [13], 7.3 b/s/Hz over 6,600 km of

Manuscript received October 6, 2017; revised November 11, 2017; accepted November 13, 2017. Date of publication December 12, 2017; date of current version February 24, 2018. *(Corresponding author: Junho Cho.)*

J. Cho, X. Chen, S. Chandrasekhar, G. Raybon, R. Dar, E. Burrows, A. Adamiecki, S. Corteselli, and P. J. Winzer are with Nokia Bell Labs, Holmdel, NJ 07733 USA (e-mail: junho.cho@nokia-bell-labs.com; xi.v.chen@nokia-bell-labs.com; Chandra.Sethumadhavan@nokia-bell-labs.com; gregory.raybon@nokia-bell-labs.com; ronen.dar@nokia-bell-labs.com; ells.burrows@nokia-bell-labs.com; andrew.adamiecki@nokia-bell-labs.com; steve.corteselli@nokia-bell-labs.com; peter.winzer@nokia-bell-labs.com).

L. Schmalen is with Nokia Bell Labs, Stuttgart 70435, Germany (e-mail: laurent.schmalen@nokia-bell-labs.com).

Y. Pan, D. Correa, B. McKay, and S. Zsigmond are with Nokia Corporation, Murray Hill, NJ 07974 USA (e-mail: yan_y.pan@nokia.com; diego.correa@nokia.com; brad.mckay@nokia.com; szilard.zsigmond@nokia.com).

S. Grubb is with Facebook, Menlo Park, CA 94025 USA (e-mail: sgrubb@fb.com).

Color versions of one or more of the figures in this paper are available online at http://ieeexplore.ieee.org.

Digital Object Identifier 10.1109/JLT.2017.2776840

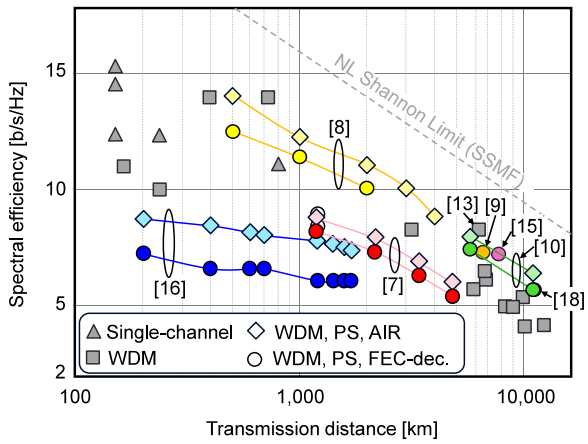

Fig. 1. Record SEs reported in literature to date.

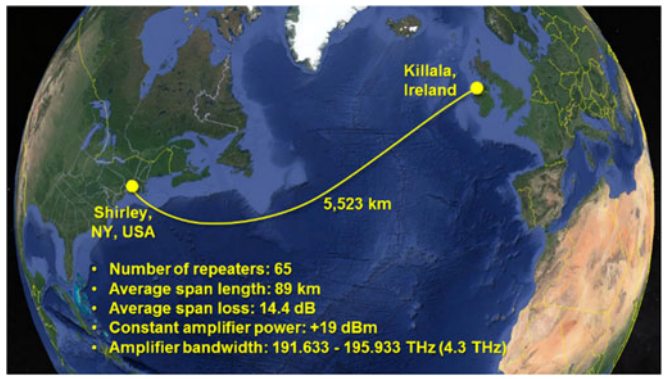

Fig. 2. Location and specification of the AEC-1 Cable.

55-km spans of 150-μm^2 effective area fiber in C+L band [9], ~6 b/s/Hz over 9,150 km of hybrid Raman/EDFA amplified 50-km spans of 134-μm^2 effective area fiber [14], and 7.23 b/s/Hz over 7,600 km of 52.8-km spans of 150-μm^2 effective area fiber in C+L band [15]. Laboratory records in terms of spectral efficiency and reach are summarized in Fig. 1, including WDM experiments (squares) and spectrally narrowly confined single-channel experiments (triangles); for the latter, the data points represent upper bounds to a potentially achievable SE.

Using PS constellations, 3 previous laboratory experiments (red [7], blue [16], and yellow [8] diamonds and circles) were used to trade off rate and reach; however, Buchali *et al.* [7] used only a single WDM channel; Yankov *et al.* [16] used five 10-GBaud signals, but on a 25-GHz grid, which leads to a significant reduction in SE compared to their reported per-channel achievable information rates ($\mathrm{AIR_{Ch}}$). Hence, as an upper bound to the potentially achievable SE performance of Refs. [7] and [16], we show in Fig. 1 their $\mathrm{AIR_{WDM}}$, i.e., their $\mathrm{AIR_{Ch}}$ scaled back by their spectral excess bandwidths, $\mathrm{AIR_{WDM}} = \mathrm{AIR_{Ch}}/(1+r)$, where r is their root raised cosine (RRC) roll-off factor (diamonds). Our laboratory results (yellow [8]) achieve record $\mathrm{AIR_{WDM}}$ over a wide range of rate/reach combinations, with $\mathrm{AIR_{WDM}}$ ranging from 14.1 b/s/Hz at 500 km to 8.9 b/s/Hz at 4,000 km. In terms of actually decoded performance, we show in Fig. 1 the (excess bandwidth corrected) scaled-back results of Refs. [7] and [16] (circles), together with our results of 12.6, 11.4, and 10.1 b/s/Hz at 500, 1,000, and 2,000 km [8]. The PS results fill the wide gap between [17], which demonstrated 14 b/s/Hz over 720 km, albeit at only 2.5 GBaud and in self-homodyne operation, and [13], which got 8.3 b/s/Hz over 6,375 km. Using geometrically shaped 32-QAM, 6.14 b/s/Hz at 11,185 km was demonstrated in C+L band in a laboratory experiment, without rate adaptability [18].

Based on the above laboratory records, we reported in [10] a field trial on the 5,523-km AEC-1 in-service, EDFA-only submarine cable consisting of 65 spans with an average length of 89 km. We demonstrated a rate-adaptable 5-carrier PS-64-QAM superchannel an off-line processed SE of 7.46 b/s/Hz on the field-deployed submarine cable, which is close to current laboratory records and suggests a capacity upgrade from the designed 13 Tb/s to 32 Tb/s per fiber on this cable. In loop-back mode, we achieved a record 5.68 b/s/Hz over 11,046 km. Using Nokia's PSE-2s digital signal processing (DSP) engine [5], we also reported a record SE of 4 b/s/Hz using real time processed 200-Gb/s and 250-Gb/s single-carrier 8-QAM and 16-QAM, thereby upgrading the capacity of the deployed submarine cable to 17.2 Tb/s per fiber with commercial margins and existing coherent transmission products. In this extended paper, we discuss in more detail our previously reported field trial results together with the underlying strategies that allowed us to achieve these record spectral efficiencies.

II. System Configuration

A. Trans-Atlantic AEC-1 Cable

The AEC-1 submarine cable connects Shirley, New York, USA, and Killala, Ireland, as shown in Fig. 2. The submarine link, built by TE Subcom and managed by AquaComms, consists of 65 spans of pure silica core fiber (Sumitomo Z+) whose effective area is 130-μm^2, and whose average loss, dispersion, and dispersion slope at 1550 nm is 0.156 dB/km, 20.5 ps/nm/km, and 0.06 ps/nm^2/km, respectively. The average span length is 89 km and the average span loss is 14.4 dB. It uses only Erbium-doped fiber amplifiers (EDFAs) of 4.3 THz bandwidth for signal amplification, ranging from 191.633 THz to 195.966 THz (extended C band) with a constant output power of 19 dBm.

B. Transponder Setup

The transmit site in Shirley, New York, contains three Nokia 500G DWDM Muxponder line cards (D5X500) [19] as part of Nokia's 1830 Photonic Service Switch (PSS) optical transport platform [20], as illustrated in Fig. 3(a). Each line card can generate two independent optical carriers that are fully tunable across the extended C band with various modulation formats [5], of which 200-Gb/s 8-QAM, 200-Gb/s and 250-GB/s 16-QAM, and 100-Gb/s QPSK (all single-carrier) were used in this trial; up to 6 modulated carriers were combined and passed through an optical line loading apparatus that used EDFAs together with wavelength-selective switches (WSS) to fill the unused system

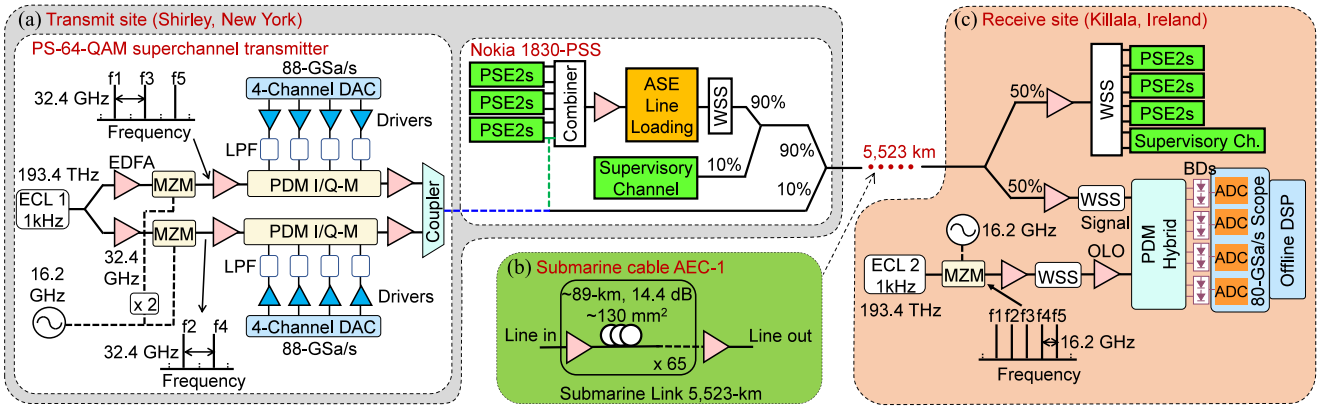

Fig. 3. Experimental setup.

bandwidth with amplified spontaneous emission (ASE) as a replacement for WDM channels. (We will discuss this line loading approach in more detail in Section II-C below.) In addition, a fourth line card that generates 32-Gbaud polarization-division multiplexed (PDM)-QPSK is used as a supervisory channel. It serves several purposes that include providing a private communication channel between the two locations as well as other functions for accessing the D5X500 channels. The respective channel under test [CUT; either a real-time D5X500 channel, indicated by the green dashed line, or an off-line PS-64-QAM superchannel, indicated by the blue dashed line in Fig. 3(a)] bypasses the line loading apparatus using a 10/90 coupler before entering the submarine link. This is done to avoid any degradation of the optical signal-to-noise ratio (OSNR) due to the line loading apparatus for the test channel.

Real-time experiments with the D5X500 channels are performed both by distributing them uniformly across the system bandwidth and by placing them next to each other at various channel spacings. For our real-time testing, a set of three 1830 PSE-2s transponders identical to those used at the transmitter serve as receivers, as shown in Fig. 3(c).

The off-line PS-64-QAM superchannel experiments use the transmitter shown in Fig. 3(a). A Redfern 1-kHz linewidth fixed-frequency external cavity laser (ECL1) at 193.4 THz is used to generate a comb of 5 carriers with 16.2-GHz spacing using sinusoidally driven Mach-Zehnder modulators (MZMs) that produce two interleaved sets of 32.4-GHz spaced tones [8]. The MZM generating the even subcarriers ($f_{2,4}$) is biased at its transmission null and driven at 16.2 GHz, and the MZM generating the odd subcarriers ($f_{1,3,5}$) is biased at quadrature and driven at 32.4 GHz. As an alternative to ECL1, we also use a line from a Roshmere narrow-linewidth comb [21], [22] at the transmitter to validate the applicability of broadband yet narrow-linewidth comb sources to higher-order modulation systems, including PS-64-QAM. No noticeable system performance difference is found between ECL1 and the comb source. Even and odd 32.4-GHz spaced carrier sets are independently modulated by $LiNbO_3$ PDM in-phase/quadrature (I/Q) modulators, driven by two 4-channel digital-to-analog converters (DACs) at 88 GSa/s to produce 16-GBd 0.01-roll-off root-raised cosine signals derived from pseudo-random bit patterns of length 3×2^{16}. The modulated signals are passively combined to form a 5-carrier superchannel.

Fig. 3(c) shows the setup of the receive site in Killala, Ireland. A second free-running ECL of the same type as ECL1 is used to generate five 16.2-GHz spaced carriers using a MZM sinusoidally driven at 16.2-GHz. A WSS selects one of the carriers as optical local oscillator (OLO) for intradyne detection. A second WSS scans through the 5 superchannel tributaries. A PDM 90° hybrid with balanced detection and 4 analog-to-digital converters (ADCs) at 80 GSa/s (Keysight 63-GHz real-time oscilloscope), acts as the coherent front-end.

C. ASE Line Loading

In submarine systems, *line loading* is important as optical amplifiers are typically operated in constant output power mode. In a fully populated system, the per-channel power is therefore given, to first order and neglecting gain tilts and channel power pre-emphasis, by the total optical amplifier power (19 dBm in our case) divided by the number of WDM channels. Test systems that do not use a fully populated set of WDM channels require loading channels to use up the remaining optical amplifier power. Several different approaches have been demonstrated in the literature to achieve such channel loading. In Refs. [13] and [15], a large bank of laser sources that cover the entire amplifier bandwidth is modulated separately from the CUT. A few others use sparsely spaced continuous wave (CW) sources over the amplifier bandwidth [11]. An alternative method is to use spectrally shaped ASE noise instead of independently modulated channels [23]–[25]. When the spectrally shaped ASE is sparse and does not fill the entire amplifier bandwidth, the nonlinear interference noise (NLIN) produced on the CUT is not the same as when the ASE fills the bandwidth completely, since NLIN from WDM channels across the entire system bandwidth plays an important role [26], [27].

In our field trial, we paid particular attention to accurately emulate a WDM system that is fully-populated with PS-64-QAM. Taking note of the fact that the complex amplitude distribution of our PS-64-QAM signal closely resembles a Gaussian optical field distribution, we chose complex Gaussian ASE as an accurate substitute for PS-64- channels.

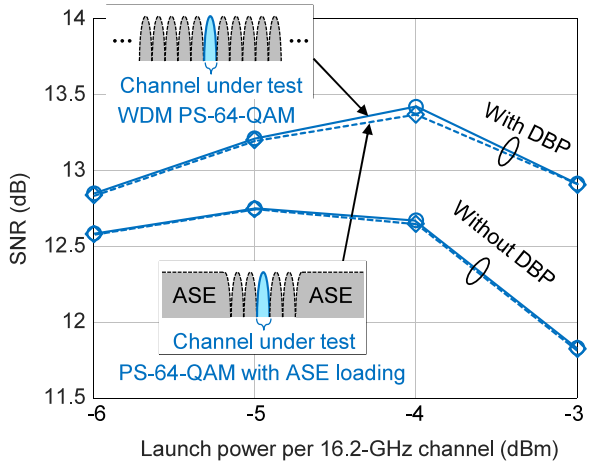

Fig. 4. Comparison of ASE line loading and fully modulated systems through split step simulations.

To ensure that ASE-based line loading indeed closely emulates a massive multiplex of modulated PS-64-QAM channels, we performed split-step simulations using the system parameters of the field-installed submarine cable, and assuming 41 PS-64-QAM WDM channels spaced at 16.2 GHz. Fig. 4 shows the recovered electrical signal-to-noise ratio (SNR) of the center carrier as a function of the launch power per 16.2-GHz channel. The solid curves represent 41 actually modulated WDM channels, while the dashed curves assume only 5 modulated center channels, replacing the remaining 18 channels to each side of the 5 modulated channels with ASE bands with a width of 18×16.2 GHz $= 291.6$ GHz each, with the same power per 16.2 GHz as the center channel. The system with ASE-based line loading exhibits almost indistinguishable performance compared to actually modulated WDM channels, both with and without single-channel digital back-propagation (DBP) for nonlinearity compensation. This quantitatively justifies our ASE-based line loading scheme as an accurate emulation of full-band WDM transmission. Note that the system bandwidth is restricted to $41 \times 16.2 \approx 664$ GHz due to the complexity of numerical split-step simulations. However, the purpose of this study is not to investigate the role of system bandwidths on NLIN but to compare ASE-based channel loading with true WDM channel loading. Fully loaded scenarios are expected to show similar results to those of Fig. 4 in terms of the difference between the SNR in systems with modulated channels and systems with ASE noise. This is particularly due to the fact that probabilistic shaping makes the per-sample distribution very close to Gaussian distribution.

In our experiments, we consequently vary the per-channel optical launch power on the AEC-1 submarine cable by altering the *system bandwidth* to preserve a constant PSD across the entire system bandwidth. This is visualized in Fig. 5: Distributing 19 dBm of constant EDFA output power across 2 THz, 2.55 THz, 3.2 THz, and 4 THz, respectively, yields -2 dBm, -3 dBm, -4 dBm, and -5 dBm per 16.2-GHz channel. This approach limits us to a minimum launch power of -5 dBm/16.2 GHz.

In order to determine the correct spectral pre-emphasis of the line loading ASE across the system bandwidth for each

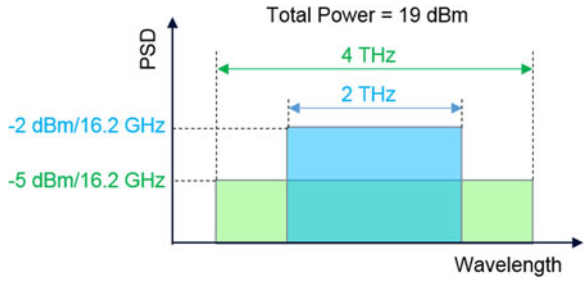

Fig. 5. Adjustment of the per-channel launch power from a constant EDFA output power.

targeted per-channel launch power, we distributed all 6 PSE-2s channels operating in 200-Gb/s 8-QAM mode across the system bandwidth and calibrated the pre-emphasis filter such that the measured real-time pre-FEC bit error ratios (BERs), expressed by their Q-factors, were within 0.1 dB of each other. The ASE was then set to fill in the gaps between the PSE-2s channels at equal PSD as smoothly as possible. The resulting optical spectra measured at transmit and receive sites are shown in Fig. 6.

III. Real-Time Transmission of Uniform QAM

Fig. 7 summarizes the real-time test results using Nokia's D5X500 line cards. A root-raised cosine roll-off factor of 0.2 was conservatively chosen throughout these tests. Using 200-Gb/s single-carrier 8-QAM on a 50-GHz grid, the trans-Atlantic link was bridged with $\sim$1.6-dB Q-factor margin at a SE of 4 b/s/Hz. Using single-carrier 16-QAM at 200 Gb/s and at 250 Gb/s, the link could still be bridged with long-term error-free real-time performance at SEs of up to 4 b/s/Hz, verified by decoding the received data for one second every 15 minutes over 8 hours, i.e., for a total of 6 to 8 Tb, corresponding to a BER below $\sim 1.6 \times 10^{-13}$. Note that these spectral efficiencies and single-carrier bit rates represent record numbers for real-time commercial coherent systems over submarine distances.

In loop-back mode, a fiber jumper at Killala directly connects the incoming signal port to the outgoing signal port without any amplification or filtering, realizing a total transmission distance of 11,046 km that is equivalent to a trans-Pacific cable. 100-Gb/s QPSK channels showed more than 3 dB of Q-factor margin (cf. Fig. 7(b); note the different reported spectral window of the loop-back results); 8-QAM channels barely missed the Q-factor threshold by $\lesssim$0.3 dB due to the insufficient time available to fine-tune various real-time coherent transponder settings.

The fact that our real-time transponder enabled trans-Pacific QPSK with excessive margin and could barely establish an 8-QAM link nicely illustrates a shortcoming of all current commercial as well as experimental transponders, i.e., the lack of fine-grained rate adaptation to maximize capacity on any given physical channel. This limitation is overcome by PS-QAM, as will be shown in the following section.

IV. Transmission of PS-64-QAM

A. PS-64-QAM With Maxwell-Boltzmann Distribution

For the off-line PS-64-QAM experiments, we used probabilistic amplitude shaping (PAS) [6] with constant composition

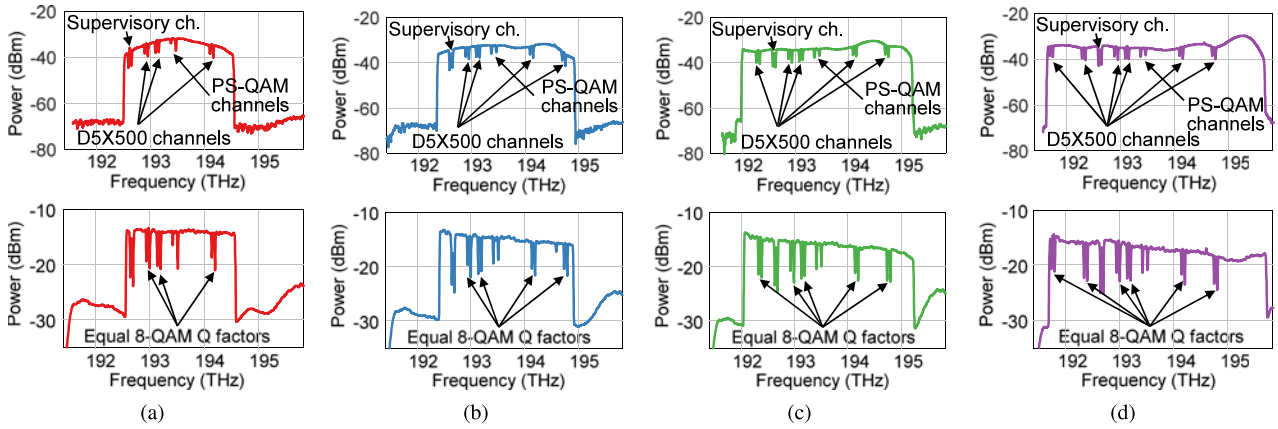

Fig. 6. Optical spectra measured with a resolution bandwidth of 0.1 nm at transmitter (upper figures) and receiver (lower figures) with system bandwidths of (a) 2 THz, (b) 2.55 THz, (c) 3.2 THz, and (d) 4 THz, that yield signal launch powers of −2 dBm, −3 dBm, −4 dBm, and −5 dBm per 16.2 GHz, respectively.

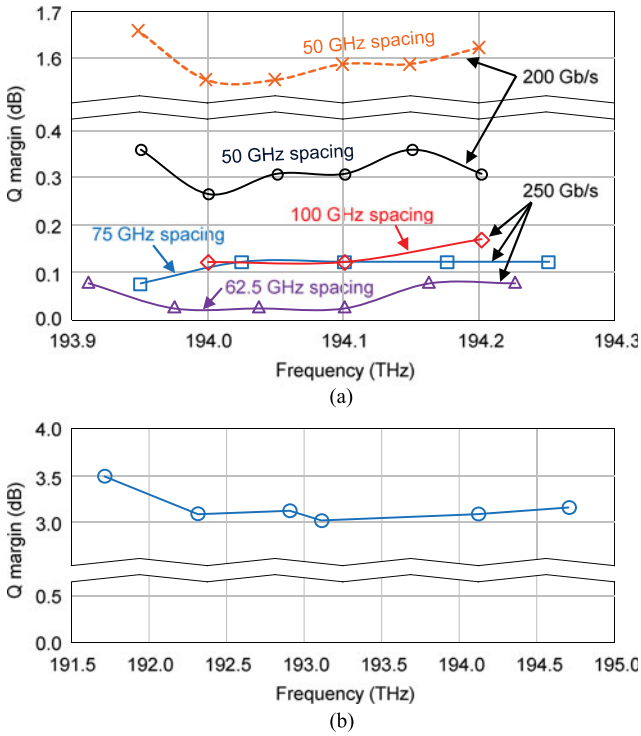

Fig. 7. Results of real-time processing: (a) with 8-QAM (dashed line) and 16-QAM (solid lines) at 5,523 km, and (b) with QPSK at 11,046 km.

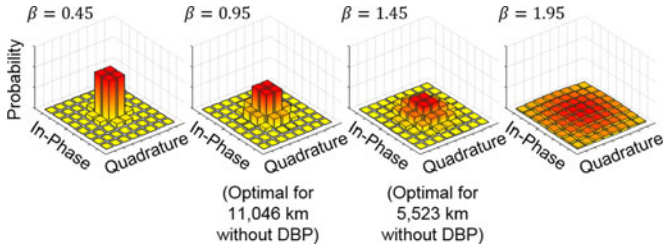

Fig. 8. Distribution of PS-64-QAM symbols with various shaping factors.

distribution matching [28] to transform a binary information bit stream into a 64-QAM symbol stream, which is considered one of the most practical implementations of probabilistic constellation shaping known to date.

It enables separate optimization of forward error correction (FEC) and PS and offers near-optimal shaping gain given by the Maxwell-Boltzmann distribution [6], [29]. The shaping factor is defined by the entropy $\beta := \mathbb{H}(\mathbf{p})$, where $\mathbf{p}$ denotes the probability mass function (PMF) of the positive half part of the constituent amplitude shift keying (ASK) constellation. For example, a PMF $\mathbf{p} := (p_1, p_2, p_3, p_4) = (0.4995, 0.3250, 0.1376, 0.0379)$ for the positive half of an 8-ASK constellation leads to a shaping factor of $\beta = \sum_{i=1}^{4} -p_i \log_2 p_i \approx 1.6$. The maximum β is $\log_2 \sqrt{M} - 1$, in which case PS-M-QAM is equivalent to uniform M-QAM. As β decreases, the PS-QAM constellation becomes Gaussian with a reduced variance. With $\beta = 0$, the constellation degenerates to QPSK. This progression is illustrated in Fig. 8. The entropy rate, which is the maximum information rate that a symbol can carry at high SNR is given for PDM PS-M-QAM as

$$\mathsf{H} = 4(1 + \beta) \quad \text{[b/symb/2-pol]}. \tag{1}$$

B. Forward Error Correction

In an auxiliary additive white Gaussian noise (AWGN) channel expressed by a conditional probability distribution $q_{Y|X}(y|x) = 1/\sqrt{2\pi\sigma^2} \cdot e^{-|y-x|^2/(2\sigma^2)}$, the *generalized mutual information (GMI)* [30] of uniform QAM under bit-metric decoding can be modified to PS-M-QAM, which can be estimated from the measured complex-valued waveform samples y_k for $k = 1, \ldots, N$ as

$$\mathsf{GMI} \approx \mathsf{H} - \frac{2}{N} \sum_{k=1}^{N} \sum_{i=1}^{m} \log_2 \frac{\sum_{x \in \chi} q_{Y|X}(y_k|x)\mathbb{P}(x)}{\sum_{x \in \chi_{b_{k,i}}} q_{Y|X}(y_k|x)\mathbb{P}(x)}, \tag{2}$$

in b/symb/2-pol, where $\mathbb{P}(x)$ denotes the probability of a symbol x, χ is the set of (single-polarization) M-QAM symbols, $b_{k,i} \in \{0, 1\}$ is the i-th bit of the k-th transmit symbol, and $\chi_{b_{k,i}}$ is the set of the M-QAM symbols whose i-th bit value is $b_{k,i}$. Note that this is termed the *bit-metric decoding rate*

in [6]. The GMI in (2) represents an *AIR* that can be achieved by ideal rate-adaptable binary FEC codes, which will generally not be the case in practice and therefore makes GMI a metric of limited relevance. Papers reporting mutual information (MI) or GMI as their final result [31]–[34] assume the existence of *ideal* FEC codes and hence give only upper bounds on the achievable performance.

In a practical scenario, given the availability of only a limited number of fixed-rate FEC codes with non-negligible implementation penalty, the IR that can actually be demonstrated with realistic FEC decoders is strictly smaller than GMI. If a code rate R_c (code overhead $1/R_c - 1$) of a practical FEC code leads to error-free decoding, the IR of the coded PS-M-QAM corresponds to

$$\mathsf{R} := \mathsf{H} - 2(1 - R_c)\log_2 M \quad \text{[b/symb/2-pol]}, \tag{3}$$

where the second term on the right-hand side is the amount of redundant information transmitted through the channel in the PAS architecture [6]. This indicates that the largest IR is achieved by using the code with the largest R_c among the set of practical FEC codes that still leads to a BER below 10^{-15}. The remaining question is then how to accurately predict from much less than 10^{15} measured bits whether a chosen practical FEC code can indeed yield a post-FEC BER below 10^{-15}. Recent studies have shown [35] that this can be done by estimating the *normalized GMI (NGMI)* from measured data, given by

$$\mathsf{NGMI} = 1 - \frac{\mathsf{H} - \mathsf{GMI}}{2\log_2 M}. \tag{4}$$

More specifically, error-free decoding can be declared if NGMI estimated from the measurement samples is larger than the threshold value $\mathsf{NGMI}^\star$ of an FEC code. This is because $\mathsf{NGMI}^\star$ is a unique characteristic quantity determined only by the underlying (practical) FEC coding scheme (i.e., an FEC code and a decoding algorithm), which provides a consistent FEC threshold across a wide range of information rates, both with and without PS [35].

In this field trial, we use *only a single FEC code*, which lets all rate adaptability be performed entirely through PS-QAM and conveniently decouples FEC code design and optimization from rate adaptation. This approach is attractive for practical ASIC implementation. In particular, we use a rate-0.8 binary spatially-coupled low-density parity-check (SC-LDPC) code (SC Code B in [36]), which has been proven through extensive field-programmable gate array (FPGA) emulation to achieve a post-FEC BER $<10^{-15}$ without an error floor within 0.94 dB of the Shannon limit on a binary-input AWGN channel with a real, fixed-point decoder with limited input and internal message resolutions. Fig. 9 shows the post-FEC BER of our SC-LDPC code as a function of the NGMI. The FPGA emulation results (circles) show that low-complexity decoding does not cause any error floor above a BER of 10^{-15}, with a decoding window of 7,500 bits $\times$ 14 copies $=$ 105,000 bits and a single decoding iteration. The software simulation results (diamonds) show that larger decoding complexity improves the waterfall performance with a decoding window of 21,850 bits $\times$ 6 copies $=$ 131,100 bits and 5 decoding iterations for the code C4 of

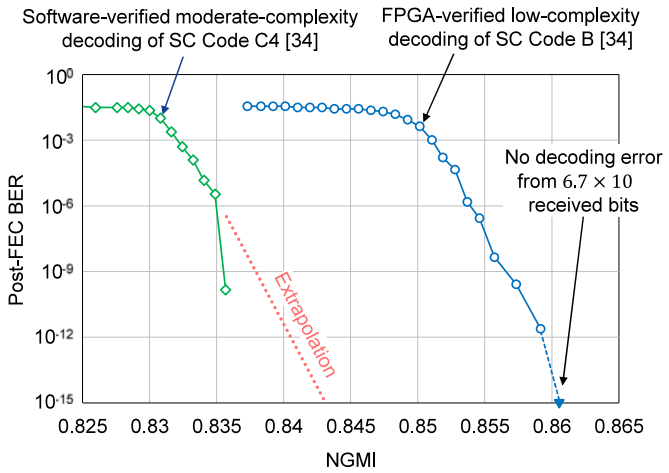

Fig. 9. Post-FEC BER of a rate-0.8 SC-LDPC code as a function of the NGMI. The dotted curve denotes extrapolation.

[36]. The former curve (solid line with circle markers) shows the NGMI threshold of $\mathsf{NGMI}^\star = 0.861$ for the FPGA-verified low-complexity SC-LDPC code, and the extrapolation of the latter curve (dotted line) provides an estimated NGMI threshold of $\mathsf{NGMI}^\star = 0.845$ for the moderate-complexity code. It is important to note in this context that a careful assessment of realistic FEC performance is key in claiming off-line transmission records that avoid unjustified over-claims.

C. Digital Signal Processing

We perform off-line coherent DSP at the receiver, individually for each 16.2-GHz optical subcarrier. The DSP consists of chromatic dispersion compensation (or single-carrier DBP using the split-step Fourier method), clock recovery, resampling the captured records of 2×10^6 samples per polarization and quadrature to 2 samples/symbol, polarization demultiplexing using an adaptive butterfly equalizer with 256 half-symbol-spaced filter taps. For polarization demultiplexing, least-mean square (LMS) equalization is pre-converged by pilots, then operated blindly. Only blindly recovered bits are used for subsequent performance assessment. The carrier phase is recovered based on the blind phase search algorithm [37].

D. Launch Power Optimization

To find the optimal launch power as a function of the PS-64-QAM shaping factor, we measure system performance at different combinations of launch powers and shaping factors. The results are shown in Fig. 10 in terms of the experimentally measured electrical symbol SNR (a, c) and the AIR (b, d), both for trans-Atlantic (a, b) and trans-Pacific (c, d) transmission scenarios. As explained above, launch powers were restricted to ≥ -5 dBm/16.2 GHz due to the fixed 19-dBm repeater output power. This also represents the best launch power we could obtain, for all shaping factors ranging from 1.1 to 1.5 at 5,523 km [see Fig. 10(a) and (b)], regardless of whether (solid) or not (dashed) single-channel DBP was employed. We see that the optimal launch power is not very sensitive to the shaping factor.

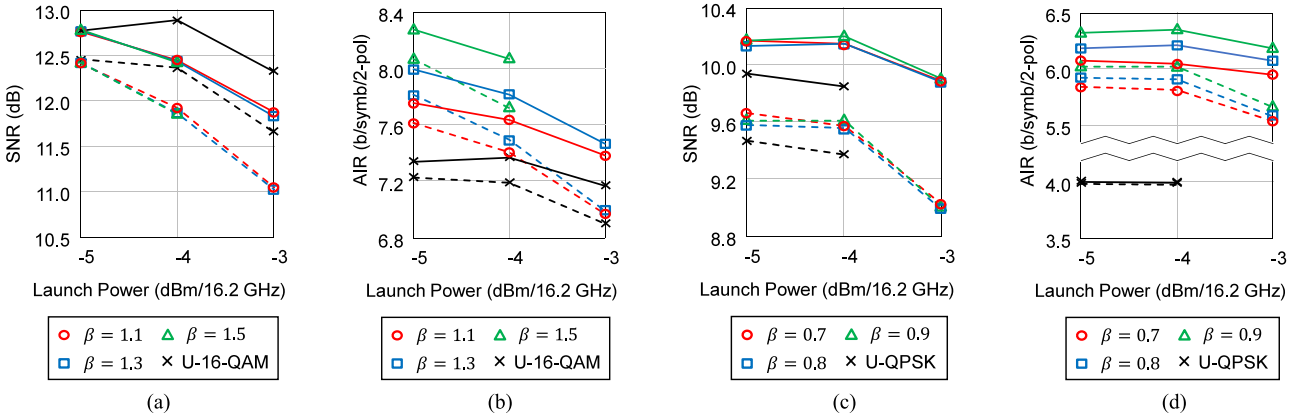

Fig. 10. SNR and AIR as a function of the launch power per 16.2 GHz at 5,523 km (a and b) and at 11,046 km (c and d). Solid and dashed lines indicate the results with and without DBP, respectively. (a) Trans-Atlantic. (b) Trans-Atlantic. (c) Trans-Pacific. (d) Trans-Pacific.

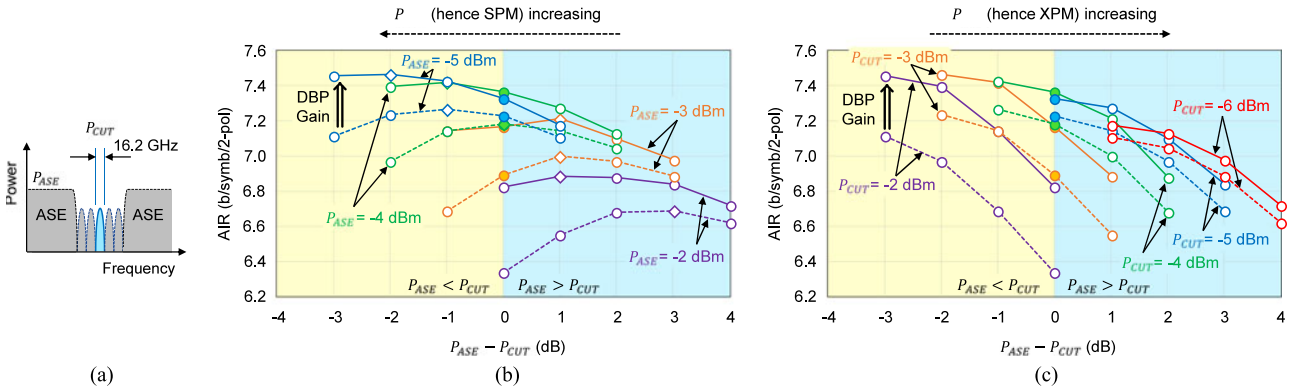

Fig. 11. AIR of U-16-QAM at 5,523 km with various power configurations: (a) illustration of the ASE power (P_{ASE}) and the CUT power (P_{CUT}), (b) AIR curves for constant P_{ASE}, and (c) AIR curves for constant P_{CUT}. Dashed and solid curves show the results without and with DBP, respectively.

With $\beta = 1.5$, and without DBP, the SNR measured in the field trial matches well the simulated SNR shown in Fig. 4, with a discrepancy of 0.29 dB at the launch power of -5 dBm/16.2 GHz. When DBP is performed, the discrepancy increases to 0.39 dB, indicating that DBP performs slightly worse in the field than what is predicted by simulations.

To assess the impact of self phase modulation (SPM) and cross phase modulation (XPM) on the AIR in more detail, we vary the optical launch power by varying the system bandwidth as before (cf. Fig. 5), and in addition we adjust the CUT power independent of the surrounding ASE power, as shown in Fig. 11(a) (Owing to experimental limitations, the two channels to each side of the CUT have the same power as the CUT.) In this set of experiments, we use uniform 16-QAM (U-16-QAM) that has a large operating margin from the channel SNR, for recovery of signals even under severe NLIN.

The measured AIRs [estimated using (2)] are visualized from two different perspectives: (i) by changing the CUT power (and the neighboring channel powers) while leaving constant the ASE power P_{ASE} [see Fig. 11(b)], and (ii) by changing the ASE power (through changing the system bandwidth) while leaving constant the CUT power P_{CUT} [and the neighboring channel powers, Fig. 11(c)]. The x-axes of these figures represent $P_{\mathrm{ASE}} - P_{\mathrm{CUT}}$ (in dB), such that 0 means $P_{\mathrm{ASE}} = P_{\mathrm{CUT}}$, negative values mean $P_{\mathrm{ASE}} < P_{\mathrm{CUT}}$ and positive values mean $P_{\mathrm{ASE}} > P_{\mathrm{CUT}}$. In all other results reported in this paper, $P_{\mathrm{CUT}} = P_{\mathrm{ASE}}$, and according to Fig. 10(b), -5 dBm/16.2 GHz and -4 dBm/16.2 GHz lead to the maximum AIRs for uniform 16-QAM, without and with single-channel DBP, respectively. The data points that also appear as black crosses in Fig. 10(b) are highlighted as solid circle markers in Fig. 11(b) and (c). At a fixed ASE power of $P_{\mathrm{ASE}} = -5$ dBm/16.2 GHz [blue curves in Fig. 11(b)], the AIR gain offered by increasing P_{CUT} is limited to 0.04 b/symb/2-pol without DBP (dashed) due to SPM. When using single-channel DBP (solid), as much as 0.14 b/symb/2-pol could be gained by increasing P_{CUT}. The same phenomenon is observed for higher ASE powers, with increasing single-channel DBP gains yet lower overall performance due to stronger XPM. Notably, although increasing the ASE power from -5 dBm/16.2 GHz to -2 dBm/16.2 GHz monotonically reduces the maximum AIR obtained from each of the optimal choices of P_{CUT} due to increasing XPM, the optimal launch power of the CUT in all cases is around -4 dBm/16.2 GHz and -3 dBm/16.2 GHz, without and with single-channel DBP, respectively. These points are indicated by diamond markers in the figure.

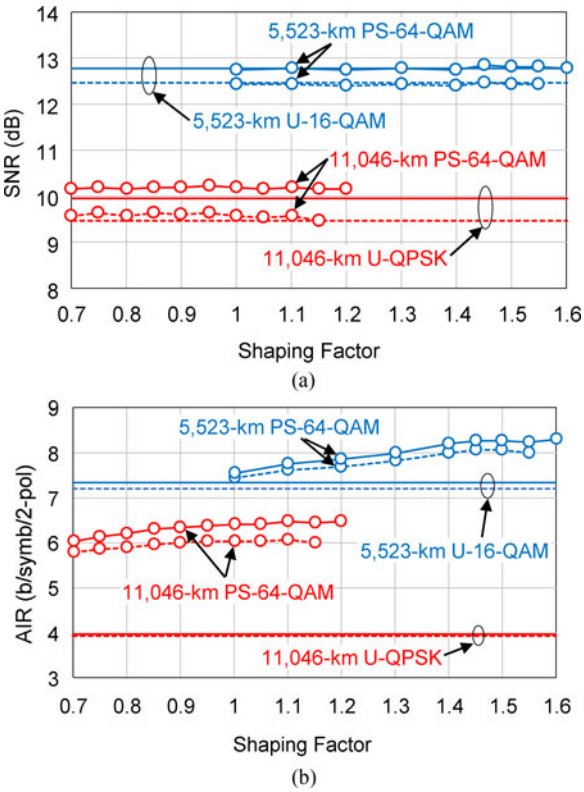

Fig. 12. SNR and AIR as a function of the shaping factor. Dashed and solid lines indicate the results without and with DBP, respectively.

Fig. 11(c) shows the same data from a different angle, keeping the power of the CUT fixed for each curve while changing the power of the ASE. This visualizes the role of XPM at constant SPM. As expected, the single-channel DBP (solid) curves run now in parallel to the curves without DBP (dashed); the gaps between them are the DBP gains, which are large for high CUT powers of $P_{\mathrm{CUT}} = -2$ dBm/16.2 GHz and small for low powers of $P_{\mathrm{CUT}} = -6$ dBm/16.2 GHz. As soon as XPM dominates SPM in terms of nonlinear distortions, we see a 0.35-b/symb/2-pol drop in AIR per dB of increased ASE power.

E. Transmission Results

For optimal rate adaptation, we measure performance metrics by varying the shaping factor in steps of 0.1 (0.05 in the region of interest).

The SNR estimated from the recovered signal is depicted in Fig. 12(a) as a function of the shaping factor β, where the results of U-16-QAM and U-QPSK are also shown for comparison. Although analytic models and simulations anticipate an SNR reduction of $\sim$0.3 dB in PS-64-QAM over 2000 km when the shaping factor decreases greatly by $\sim$1.67 [38], our field trial yields constant SNR within measurement accuracies, despite a change of the shaping factor by 0.6.

The measured GMI, which is an AIR in our system configuration[1], is shown in Fig. 12(b), where it can be seen

[1]GMI and MI, respectively, represent AIRs under bit-metric decoding and symbol-metric decoding.

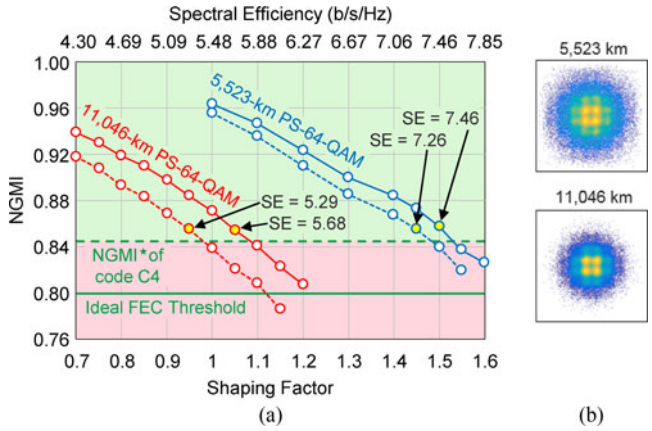

Fig. 13. (a) NGMI measured at the center channel, and (b) typical recovered constellations.

that the AIR increases with increasing shaping factor β. In principle, one should expect a single maximum in the AIR as a concave function of β, at some optimal value β^* for which the shaped PMF is ideally matched to the underlying auxiliary AWGN channel. However, when gradually increasing β in the field trial, i.e., reducing the shaping and more closely approaching a uniform 64-QAM constellation, we found that the coherent DSP gradually fails to robustly recover the received signals, hence the decrease of AIR was not observed. This is because a more uniform PS constellation has a smaller minimum Euclidean distance between constellation symbols for the same average power. Therefore, for a given noise power, the performance of those DSP functions that rely on symbol decisions, such as the LMS equalization, can deteriorate as the constellation becomes more uniform. This practical aspect of PS nicely reveals that implementation penalties, both from hardware imperfections and from DSP and coding imperfections, cannot be neglected in optimizing a PS system.

In Fig. 12(b), at 5,523 km, the gain in AIR due to PS-64-QAM relative to uniform QAM amounts to 0.84 b/symb/2-pol and 0.97 b/symb/2-pol, without and with DBP, respectively, thereby achieving 12% to 13%-larger AIRs. At 11,046 km, the gain is significantly larger, reaching 2.13 b/symb/2-pol and 2.5 b/symb/2-pol, without and with DBP, respectively. This is because the AIR of U-QPSK is saturated almost at its entropy rate with a large SNR margin with a negligible FEC overhead (OH), suggesting that U-16-QAM with a greater FEC OH will yield a better AIR, which however could not be implemented due to unstable coherent DSP for U-16-QAM. As a consequence, 54% to 63%-larger AIRs were achieved by using rate-adaptable PS-QAM compared to uniform QAM.

The NGMI measured on the AEC-1 cable is shown in Fig. 13(a). The net SE on the top horizontal axis can be directly calculated from β and (1) and (3) as $\mathsf{SE} = \mathsf{R} \cdot 16\ \mathrm{GHz}/16.2\ \mathrm{GHz}$, by taking into account the 25% FEC OH and the 16.2-GHz WDM channel spacing. With moderate-complexity SC-LDPC coding, the largest shaping factors that lead to $\mathsf{NGMI} > \mathsf{NGMI}^\star$, and hence realistically error-free decodable performance, are 1.45 (5,523 km), 1.5 (5,523 km with

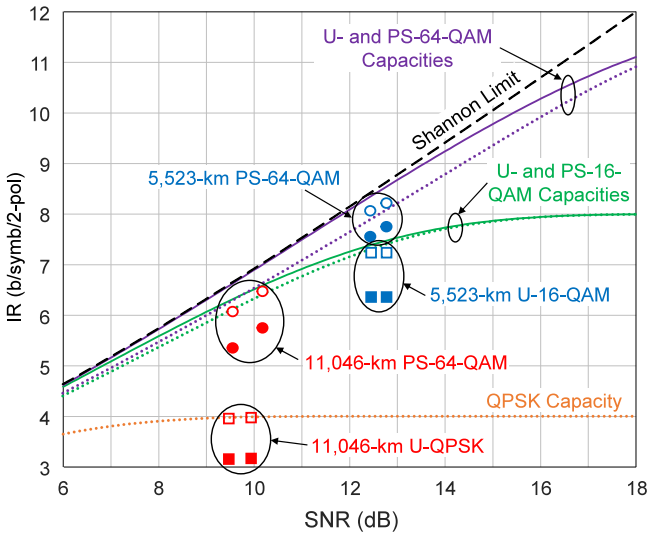

Fig. 14. AIRs (open markers) and actually achieved IRs (closed markers) with U-QAM and PS-QAM. Left and right markers in each pair of markers indicate the results obtained without and with DBP, respectively. Dotted and solid lines denote U-QAM and PS-QAM capacities in AWGN, respectively.

DBP), 0.95 (11,046 km), and 1.05 (11,046 km with DBP), with the corresponding SEs of 7.26, 7.46, 5.29, and 5.68 b/s/Hz. With low-complexity SC-LDPC coding as verified by FPGA emulation, the SEs are reduced by 0.2 b/s/Hz for all cases, which amount to 7.06, 7.26, 5.09, and 5.48 b/s/Hz, respectively. The net SEs of uniform modulations correspond to 6.32 b/s/Hz (U-16-QAM) and 3.16 b/s/Hz (U-QPSK), respectively, at 5,523 km and 11,046 km. The 5 superchannel tributaries show uniformly good performance with NGMIs between 0.851 and 0.86 (averaged to 0.854), greater than $\mathsf{NGMI}^{\star} = 0.845$ for the moderate-complexity SC-LDPC code. We actually decoded the measured data individually and jointly, and found error-free performance.

The AIRs and the IRs that are achieved with our SC-LDPC code at optimum shaping factors with PS-64-QAM, and those of U-QPSK and U-16-QAM are plotted in Fig. 14 as a function of SNR, with reference to theoretic capacities in the AWGN channel, where the SNR is estimated from the recovered constellations using the mean squared error between the transmitted and the corresponding received symbols. With respect to the AIRs, PS-64-QAM approaches the Shannon limit to within 0.5 dB (at 5,523 km) and 1 dB (at 11,046 km), while U-QAM produces a huge gap of 2.2 dB (at 5,523 km) and 5 dB (at 11,046 km), when DBP is performed. In terms of the actually achieved IRs with our practical SC-LDPC code, PS-64-QAM has a gap of 1.4 dB (at 5,523 km) and 2.3 dB (at 11,046 km), and U-QAM has a gap of 3.7 dB (at 5,523 km) and 6.5 dB (at 11,046 km).

V. Conclusion

In this paper, we demonstrated record or near-record SEs of 7.46 and 5.68 b/s/Hz at transmission distances of 5,523 and 11,046 km, respectively, using PS 64-QAM in a field trial on an in-service trans-Atlantic fiber-optic cable. Compared to uniform square QAM, the field trial results achieved 18% and 80% increases of SE in carefully emulated full C-band DWDM transmission. We also demonstrated record real-time coherent transmission of single-carrier 200-Gb/s and 250-Gb/s uniform 8-QAM and 16-QAM at 4 b/s/Hz over the 5,523-km cable.

We introduced a systematic approach to optimizing the underlying PS-QAM by finding the maximum shaping factor that leads to the greatest IR and SE under an actually implementable fixed-rate FEC coding scheme, where error-free FEC decoding was accurately examined by the NGMI threshold. With this optimization of coded modulation, we showed that our field trial results approached the Shannon limit to within 1.4 and 2.3 dB at 5,523 and 11,046 km, respectively, with a practical FEC coding scheme.

References

[1] P. J. Winzer and D. T. Neilson, "From scaling disparities to integrated parallelism: A decathlon for a decade," *J. Lightw. Technol.*, vol. 35, no. 5, pp. 1099–1115, Mar. 2017.

[2] Y. Sverdlik, "Here are the submarine cables funded by cloud giants," Mar. 2017. [Online]. Available: http://www.datacenterknowledge.com/archives/2017/03/03/here-are-the-sub marine-cables-funded-by-cloud-giants/

[3] Aqua Comms Limited, "AEConnect—The newest, most secure Transatlantic cable system in existence." [Online]. Available: http://www.aquacomms.com/networks/aec-america-europe-connect, Accessed on: Nov. 27, 2017.

[4] A. Pilipetskii, "High capacity submarine transmission systems," in *Proc. Opt. Fiber Commun. Conf.*, 2015, Paper W3G.5.

[5] Nokia Corporation, "The photonic service engine 2." [Online]. Available: https://resources.ext.nokia.com/asset/194079, Accessed on: Nov. 27, 2017.

[6] G. Böcherer, F. Steiner, and P. Schulte, "Bandwidth efficient and rate-matched low-density parity-check coded modulation," *IEEE Trans. Commun.*, vol. 63, no. 12, pp. 4651–4665, Dec. 2015.

[7] F. Buchali, F. Steiner, G. Böcherer, L. Schmalen, P. Schulte, and W. Idler, "Rate adaptation and reach increase by probabilistically shaped 64-QAM: An experimental demonstration," *J. Lightw. Technol.*, vol. 34, no. 7, pp. 1599–1609, Apr. 2016.

[8] S. Chandrasekhar *et al.*, "High-spectral-efficiency transmission of PDM 256-QAM with parallel probabilistic shaping at record rate-reach trade-offs," in *Proc. Eur. Conf. Opt. Commun.*, 2016, Paper Th.3.C.1.

[9] A. Ghazisaeidi *et al.*, "65 Tb/s transoceanic transmission using probabilistically-shaped PDM-64QAM," in *Proc. Eur. Conf. Opt. Commun.*, 2016, Paper Th.3.C.4.

[10] J. Cho *et al.*, "Trans-Atlantic field trial using probabilistically shaped 64-QAM at high spectral efficiencies and single-carrier real-time 250-Gb/s 16-QAM," in *Proc. Opt. Fiber Commun. Conf.*, 2017, Paper Th5B.3.

[11] V. A. J. M. Sleiffer *et al.*, "45.8 and 125 Gb/s CP-QPSK/CP-BPSK field trial over installed submarine cable," *J. Lightw. Technol.*, vol. 30, no. 5, pp. 624–633, Feb. 2012.

[12] K. Wang, Y. Lu, and L. Liu, "Dual-carrier 400G field trial submarine transmission over 6,577-km using 60-GBaud digital faster-than-Nyquist shaping PDM-QPSK modulation format," in *Proc. Opt. Fiber Commun. Conf.*, 2015, Paper W3E.2.

[13] S. Zhang *et al.*, "Capacity-approaching transmission over 6375 km at spectral efficiency of 8.3 bit/s/Hz," in *Proc. Opt. Fiber Commun. Conf.*, 2016, Paper Th5C.2.

[14] J.-X. Cai *et al.*, "49.3 Tb/s transmission over 9100 km using C+L EDFA and 54 Tb/s transmission over 9150 km using hybrid-Raman EDFA," *J. Lightw. Technol.*, vol. 33, no. 13, pp. 2724–2734, Jul. 2015.

[15] J.-X. Cai *et al.*, "70.4 Tb/s capacity over 7,600 km in C+L band using coded modulation with hybrid constellation shaping and nonlinearity compensation," in *Proc. Opt. Fiber Commun. Conf.*, 2017, Paper Th5B.2.

[16] M. P. Yankov *et al.*, "Constellation shaping for WDM systems using 256QAM/1024QAM with probabilistic optimization," *J. Lightw. Technol.*, vol. 34, no. 22, pp. 5146–5156, Nov. 2016.

[17] T. Omiya, M. Yoshida, and M. Nakazawa, "400 Gbit/s 256 QAM-OFDM transmission over 720 km with a 14 bit/s/Hz spectral efficiency by using high-resolution FDE," *Opt. Express*, vol. 21, no. 3, pp. 2632–2641, Feb. 2013.

[18] S. Zhang *et al.*, "50.962 Tb/s over 11185 km bi-directional C+L transmission using optimized 32QAM," in *Proc. Conf. Lasers Electro-Opt.*, 2017, Paper JTh5A.9.
[19] Nokia Corporation, "Nokia 1830 PSS 500G muxponder." [Online]. Available: https://resources.ext.nokia.com/asset/194076, Accessed on: Nov. 27, 2017.
[20] Nokia Corporation, "Nokia 1830 PSS-24x." [Online]. Available: https://resources.ext.nokia.com/asset/194070, Accessed on: Nov. 27, 2017.
[21] Roshmere Inc., White Paper. [Online]. Available: http://roshmere.com/white-paper/, Accessed on: Nov. 27, 2017.
[22] B. J. Puttnam *et al.*, "2.15 Pb/s transmission using a 22 core homogeneous single-mode multi-core fiber and wideband optical comb," in *Proc. Eur. Conf. Opt. Commun.*, 2015, Paper PDP.3.1.
[23] M. E. McCarthy, N. M. Suibhne, S. T. Le, P. Harper, and A. D. Ellis, "High spectral efficiency transmission emulation for non-linear transmission performance estimation for high order modulation formats," in *Proc. Eur. Conf. Opt. Commun.*, 2014, Paper P.5.7.
[24] D. J. Elson, L. Galdino, R. Maher, R. I. Killey, B. C. Thomsen, and P. Bayvel, "High spectral density transmission emulation using amplified spontaneous emission noise," *Opt. Lett.*, vol. 41, no. 1, pp. 68–71, 2016.
[25] D. S. Millar *et al.*, "A simplified dual-carrier DP-64QAM 1 Tb/s transceiver," in *Proc. Opt. Fiber Commun. Conf.*, 2017, Paper M3D.2.
[26] R. Dar and P. J. Winzer, "On the limits of digital back-propagation in fully loaded WDM systems," *IEEE Photon. Technol. Lett.*, vol. 28, no. 11, pp. 1253–1256, Jun. 2016.
[27] R. Dar and P. J. Winzer, "Nonlinear interference mitigation: Methods and potential gain," *J. Lightw. Technol.*, vol. 35, no. 4, pp. 903–930, Feb. 2017.
[28] P. Schulte and G. Böcherer, "Constant composition distribution matching," *IEEE Trans. Inf. Theory*, vol. 62, no. 1, pp. 430–434, Jan. 2016.
[29] F. R. Kschischang and S. Pasupathy, "Optimal nonuniform signaling for Gaussian channels," *IEEE Trans. Inf. Theory*, vol. 39, no. 3, pp. 913–929, May 1993.
[30] A. Alvarado, E. Agrell, R. Maher, and P. Bayvel, "Replacing the soft FEC limit paradigm in the design of optical communication systems," *J. Lightw. Technol.*, vol. 34, no. 2, pp. 4338–4352, Oct. 2016.
[31] T. A. Eriksson, F. Buchali, W. Idler, L. Schmalen, and G. Charlet, "Electronically subcarrier multiplexed PM-32QAM with optimized FEC overheads," in *Proc. Opt. Fiber Commun. Conf.*, 2017, Paper W3J.4.
[32] F. Buchali, W. Idler, L. Schmalen, and Q. Hu, "Flexible optical transmission close to the Shannon limit by probabilistically shaped QAM," in *Proc. Opt. Fiber Commun. Conf.*, 2017, Paper M3C.3.
[33] F. Buchali, W. Idler, L. Schmalen, G. Böcherer, P. Schulte, and F. Steiner, "Probabilistically shaped QAM for independent reach, spectral efficiency and bit-rate adaptation," in *Proc. Eur. Conf. Opt. Commun.*, 2016, Paper W.1.C.1.
[34] M. P. Yankov *et al.*, "Experimental study of nonlinear phase noise and its impact on WDM systems with DP-256QAM," in *Proc. Eur. Conf. Opt. Commun.*, 2016, Paper W.1.D.1.
[35] J. Cho, L. Schmalen, and P. J. Winzer, "Normalized generalized mutual information as a forward error correction threshold for probabilistically shaped QAM," in *Proc. Eur. Conf. Opt. Commun.*, 2017, Paper M.2.D.2.
[36] L. Schmalen, V. Aref, J. Cho, D. Suikat, D. Rösener, and A. Leven, "Spatially coupled soft-decision error correction for future lightwave systems," *J. Lightw. Technol.*, vol. 33, no. 5, pp. 1109–1116, Mar. 2015.
[37] T. Pfau, S. Hoffmann, and R. Noé, "Hardware-efficient coherent digital receiver concept with feedforward carrier recovery for M-QAM constellations," *J. Lightw. Technol.*, vol. 27, no. 8, pp. 989–999, Apr. 2009.
[38] T. Fehenberger, A. Alvarado, G. Böcherer, and N. Hanik, "On probabilistic shaping of quadrature amplitude modulation for the nonlinear fiber channel," *J. Lightw. Technol.*, vol. 34, no. 21, pp. 5063–5073, Nov. 2016.

Junho Cho received the B.S., M.S., and Ph.D. degrees in electrical engineering and computer science from Seoul National University, Seoul, South Korea. Since 2010, he has been with Bell Laboratories, Holmdel, NJ, USA, as a member of technical staff. He was a Ph.D. dissertation committee member for Seoul National University. He has authored or coauthored numerous papers and was a Reviewer for a wide range of IEEE journals, the scope of which includes the optics, communications, circuits and systems, and computer. His current research interests include probabilistic constellation shaping, forward error correction, and signal processing. He was the recipient of the Outstanding Research Award under the Brain Korea 21 Project while studying with Seoul National University in 2009, and the Outstanding Reviewer Award from the IEEE/OSA JOURNAL OF LIGHTWAVE TECHNOLOGY in 2017.

Xi Chen received the B.E. degree in telecommunication engineering from the National University of Defense Technology, Changsha, China, in 2008, and the Ph.D. degree from the University of Melbourne, Melbourne, VIC, Australia, in 2012. In 2008, she was with Huaweis Wireless Networking Department, and from 2013 to 2015, he was a Research Fellow in the University of Melbourne, conducting research on optical fiber transmission. Since 2015, she has been with Nokia Bell Labs, Holmdel, NJ, USA. Her current research interest includes advanced digital signal processing for high-speed optical subsystems and fiber transmission.

Sethumadhavan Chandrasekhar (F'01) received the Ph.D. degree in physics from the University of Bombay, Mumbai, India, in 1985. From 1975 to 1985, he was with the Tata Institute of Fundamental Research, Bombay, India. In 1986, he joined AT&T Bell Laboratories (now called Nokia Bell Labs), Crawford Hill Laboratory, Holmdel, NJ, USA. He initially worked on compound semiconductor devices and high-speed optoelectronic integrated circuits (OEICs). Since 1999, he has been responsible for forward looking research in WDM optical networking at 40 Gb/s, 100 Gb/s, and beyond 100 Gb/s. He holds more than 35 U.S. patents and has authored or coauthored more than 250 peer-reviewed journal articles. His current interests include coherent optical transmission systems for high spectral efficiency transport and networking beyond 100 Gb/s, multicarrier superchannels, and software-defined transponders for efficient end-to-end optical networking. He is a Fellow of the Optical Society of America and Nokia Bell Labs. He was as an Associate Editor for ten years for the IEEE PHOTONICS TECHNOLOGY LETTERS, and is currently an Associate Editor for *Optics Express*. He was the recipient of the IEEE LEOS Engineering Achievement Award in 2000 and the OSA Engineering Excellence Award in 2004 for his contributions to OEICs and WDM systems research.

Gregory Raybon (F'16) received the B.S. degree in electrical engineering from Pennsylvania State University, State College, PA, USA, in 1984, the M.S. degree in material science from Stevens Institute of Technology, Hoboken, NJ, USA, in 1989. He is a member of technical staff with Nokia Bell Labs, Holmdel, NJ, USA. High-speed optical transmission systems have been the focus of his research since a record-breaking 8 Gb/s optical time-division multiplexing transmission system in 1988. Today the research continues on coherent optical transmission systems approaching speeds of 1 Tb/s achieved through advances in high-speed electrical and optoelectrical components. He is a Fellow of the OS.

Ronen Dar received the B.Sc. (*cum laude*), M.Sc. (*summa cum laude*), and Ph.D. degrees in electrical engineering from Tel-Aviv University, Tel-Aviv, Israel, in 2008, 2011, and 2015, respectively. He is a member of technical staff in the Optical Transmission Systems and Networks Research Department, Nokia Bell Labs, Holmdel, NJ, USA. During 2006–2008, he was an Algorithm Engineer in Intels Mobile Wireless Group, and during 2008–2015, in Anobit Technologies, a developer of advanced signal processing solutions for the storage markets (acquired by Apple Inc. in 2011). He is a coauthor of several patents in the fields of communication, signal processing, and coding. He was the recipient of the Adams Fellowship awarded by the Israeli Academy of Sciences and Humanities (2013–2015), the Advanced Communication Center Award of TelAviv University for outstanding research work in the field of communications (2014), the Electro-Optic Fund Award of Tel-Aviv University for outstanding research work (2014), and the Weinstein Award for outstanding publications in the fields of signal processing and communication (2013 and 2014).

Laurent Schmalen received the Dipl.Ing. degree in electrical engineering and information technology and the Dr.Ing. degree from the RWTH Aachen University of Technology, Aachen, Germany. In 2011, he joined Bell Labs, Stuttgart, Germany, as a member of technical staff where he is currently the Head of the Department of Coding in Optical Communications, IP and Optical Transport Research Laboratory. Since 2014, he has been the Guest Lecturer with the University of Stuttgart, Stuttgart, Germany. His research interests include forward error correction, modulation formats, and information theory for future optical networks. He was a two-time recipient of the Friedrich-Wilhelm Award, and the E-Plus Award for his Ph.D. thesis. He was also the recipient of the Best Paper Award of the 2010 ITG Speech Communication Conference, the 2013 Best Student Paper Award at the IEEE Signal Processing Systems workshop, and the 2014 IEEE Transactions on Communications Exemplary Reviewer Award.

Ells Burrows is a member of technical staff with Nokia Bell Labs, Holmdel, NJ, USA.

Andrew Adamiecki received the B.S. and M.S. degrees in electrical engineering from the Silesian University of Technology, Gliwice, Poland. He is a member of technical staff with the Photonics Research Department, Nokia Bell Labs, Holmdel, NJ, USA. Prior to his tenure at Bell Labs, he was a senior RF Communications Engineer with Ademco, a division of Pittway Corporation, Syosset, NY, USA, working on direct sequence spread spectrum techniques for commercial security system applications. He then joined AT&Ts Consumer Product Division working on GSM and CDMA based cellular phone architectures. In 2001, he joined Bell Labs Optical/Data Networking Research Department working on signal integrity for high-speed data transmission over electrical backplanes and 40 Gb/s electro-optic integrated circuit design. His current research interests include 100 Gb/s electro-optic packaging techniques, microwave, and high-speed electronics circuit development for terabit transmission optical networks.

Steve Corteselli is a research engineer with Nokia Bell Labs, Holmdel, NJ, USA.

Yan Pan is a member of Nokia IP Transport Business Unit.

Diego Correa is a member of Nokia IP Transport Business Unit.

Brad McKay is a technical manager with Nokia IP Transport Business Unit.

Szilard Zsigmond received the Ph.D. degree from the Budapest University of Technology and Economics, Tokyo, Japan. He is a Principal Product Line Manager of photonic line systems, amplifiers, and node configurations with Nokia, Espoo, Finland. He is also the Product Line Manager of Terrestrial-Subsea Integration, Nokia. He has extensive knowledge of optical communication systems and expertise of fiber-optics communication. Prior to Nokia, he was a Researcher and a Lecturer with the Budapest University of Technology and Economics. He was also a Visiting Researcher with the National Institute of Information and Communications Technology, Tokyo, Japan. In 2010, he joined Alcatel-Lucent where he was responsible for transport solutions and business development in central and north-east region of Europe. In 2012, he became the Solution Architect of Asia–Pacific region and later became the Head of Asia–Pacific Regional Product Line Management. In 2014, he joined the core Product Line Management team being the Principal Product Line Manager of photonic line systems. He has numerous speaking in various conferences and has authored or coauthored more than 40 scientific papers.

Peter J. Winzer (F'09) received the Ph.D. degree from the Vienna University of Technology, Vienna, Austria, where he worked on space-borne lidar and laser communications for the European Space Agency. Since 2000, he has been with Bell Labs, Holmdel, NJ, USA, and has focused on many aspects of fiber-optic communications and networking, from advanced optical modulation, multiplexing, and detection to cross-layer network architectures. He has contributed to several high-speed optical transmission records from 100 Gb/s to 1 Tb/s in laboratory experiments and field trials, and has been widely promoting spatial multiplexing to overcome the optical networks capacity crunch. He has amply authored or coauthored and patented, and is actively involved with the IEEE Photonics Society and the Optical Society of America, including service as the Program Chair of ECOC 2009, Program/General Chair of OFC 2015/17, and the current Editor-in-Chief for the IEEE/OSA JOURNAL OF LIGHTWAVE TECHNOLOGY. He was the recipient of multiple awards for his work and is a highly cited researcher. He is a Fellow of Bell Labs and the OSA, and an elected member of the U.S. National Academy of Engineering.

Steve Grubb received the Ph.D. degree from Cornell University, Ithaca, NY, USA. He is currently a Global Optical Architect with Facebook, Menlo Park, CA, USA, overseeing the build of several new open submarine cable systems and introducing new optical technologies for Facebook's global network. Prior to Facebook, he was a Fellow at Infinera where for 14 years he directed work on next generation photonic integrated optical and network technologies. He was also responsible for the first commercial introduction of Raman amplifiers in fiber networks. He demonstrated and patented several unique laser and amplifier devices while at Bell Labs, including the cascaded Raman resonator. He has more than 120 published papers and conference contributions and more than 75 issued U.S. patents.